

See discussions, stats, and author profiles for this publication at: <https://www.researchgate.net/publication/256612755>

Exploring Supramolecular Self-Assembly of Tetraarylporphyrins by Halogen Bonding: Crystal Engineering with Diversely Functionalized Six-Coordinate Tin(L)(2)-Porphyrin Tectons

ARTICLE *in* CHEMISTRY - A EUROPEAN JOURNAL · OCTOBER 2013

Impact Factor: 5.73 · DOI: 10.1002/chem.201301857 · Source: PubMed

CITATIONS

13

READS

20

3 AUTHORS, INCLUDING:



Ranjan Patra

Atomic Energy and Alternative Energies Co...

22 PUBLICATIONS 313 CITATIONS

SEE PROFILE

Exploring Supramolecular Self-Assembly of Tetraarylporphyrins by Halogen Bonding: Crystal Engineering with Diversely Functionalized Six-Coordinate $\text{Sn}(\text{L})_2$ -Porphyrin Tectons

Hatem M. Titi, Ranjan Patra, and Israel Goldberg*^[a]

Abstract: This study targets the construction of porphyrin assemblies directed by halogen bonds, by utilizing a series of purposely synthesized $\text{Sn}(\text{axial ligand})_2$ -(5,10,15,20-tetraarylporphyrin) [$\text{Sn}(\text{L})_2\text{-TArP}$] complexes as building units. The porphyrin moiety and the axial ligands in these compounds contain different combinations of complementary molecular recognition functions. The former bears *p*-iodophenyl, *p*-bromophenyl, 4'-pyridyl, or 3'-pyridyl substituents at the *meso* positions of the porphyrin ring. The latter comprises either a carboxylate or hydroxy anchor for attachment to the porphyrin-

in-inserted tin ion and a pyridyl-, benzotriazole-, or halophenyl-type aromatic residue as the potential binding site. The various complexes were structurally analyzed by single-crystal X-ray diffraction, accompanied by computational modeling evaluations. Halogen-bonding interactions between the lateral aryl substituents of one unit of the porphyrin complex and the axial ligands of neighboring moieties was suc-

cessfully expressed in several of the resulting samples. Their occurrence is affected by structural (for example, specific geometry of the six-coordinate complexes) and electronic effects (for example, charge densities and electrostatic potentials). The shortest intermolecular I...N halogen-bonding distance of 2.991 Å was observed between iodo-phenyl (porphyrin) and benzotriazole (axial ligand) moieties. Manifestation of halogen bonds in these relatively bulky compounds without further activation of the halophenyl donor groups by electron-withdrawing substituents is particularly remarkable.

Keywords: halogens • porphyrins • self-assembly • supramolecular chemistry • tin


Introduction

Halogen bonds are attractive noncovalent supramolecular interactions for the rational design of new crystalline materials.^[1–3] Various applications of halogen bonding have been reviewed recently,^[2,3] and these include the production of supramolecular nanowires, supramolecular gel formation, production of liquid crystals, and crystal engineering.^[4,5] The common halogen-bonding interaction can be explained by electrostatic terms because it involves the positive electrostatic potential of the halogen atom and an electron-rich atom (for example, N, O, I, or Br) that acts as a Lewis base. Halogen interactions are specific and directional, and they have been proven to play a crucial role in crystalline materials.^[1–5] Investigation of the various and articulated halogen-bonding schemes in porphyrins offers a new challenge in crystal engineering. Porphyrin compounds are important entities in materials chemistry because of their unique photo-

chemical, catalytic, and electronic properties,^[6] and they are particularly interesting from a functional point of view. When suitably “activated” by complementary molecular recognition functions, they represent ideal organic building blocks for the designed construction of extended supramolecular architectures.^[7] Chemical modifications can be readily performed both in the core and on the porphyrin periphery, as well as by the addition of reactive axial ligands bound to the metal centers with preferred five- or six-coordination features.^[7,8] A wide variety of novel porphyrin-based supramolecular architectures assembled primarily through intermolecular coordination and hydrogen-bonding interactions has been reported in recent years. Programmed functionalization of tetraarylporphyrin building blocks has led in recent years to the discovery by others and us of a large number of supramolecular porphyrin-based networks and frameworks, formed by direct interporphyrin hydrogen bonding and coordination or tessellated by external metal-ion or organic-ligand bridging auxiliaries.^[7–11] Some of these tunable heterometallic frameworks constructed from paddle-wheel-type dinuclear metal-ion connectors, and with open access to the porphyrin metal centers, can be particularly useful for heterogeneous-catalysis applications^[11] and as active materials for visible-light catalysis.^[12] Recent work in this area also involves highly stable mesoporous metalloporphyrin frameworks tessellated by polynuclear zirconium-ion clusters, which are of potential utility in biomimetic catalysis^[13] and as permanently microporous materials with se-

[a] H. M. Titi,* Dr. R. Patra,* Prof. I. Goldberg
School of Chemistry, Sackler Faculty of Exact Sciences
Tel-Aviv University, Ramat-Aviv, 69978 Tel-Aviv (Israel)
E-mail: goldberg@post.tau.ac.il

[*] These authors contributed equally to this work.

 Supporting information for this article is available on the WWW under <http://dx.doi.org/10.1002/chem.201301857>. It contains X-ray crystallographic details in CIF format for compounds **1–9** and experimental data and additional figures and tables related to the computational modeling.

lective carbon dioxide uptake.^[14] The formation of hybrid metalloporphyrin frameworks not only in crystalline bulk but also as highly crystalline nanofilms on surfaces has been reported as well.^[15] On the other hand, multiporphyrin assembly with the aid of halogen bonds has received only minor attention until now. In a number of pioneering reports on this subject, we have demonstrated the effectiveness of I...N and Br...N halogen bonds in directing the self-organization of porphyrin entities in crystals.^[16] Porphyrin units with mixed *meso* substitutions of 4-pyridyl and either 4-iodo- or 4-bromophenyl residues have been used to this end, which has resulted in the formation of halogen-bonded layered assemblies (Figure 1). Moreover, asymmetric substitution of the porphyrin scaffolds led to the formation of chiral architectures.

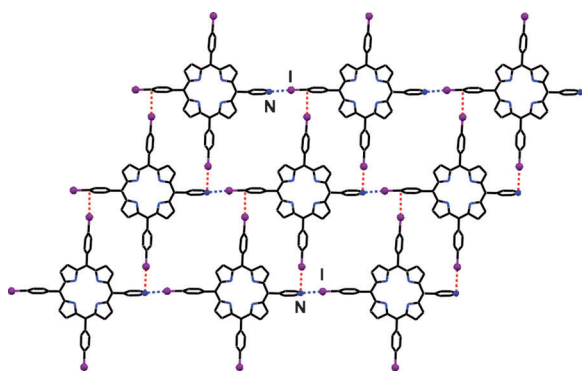
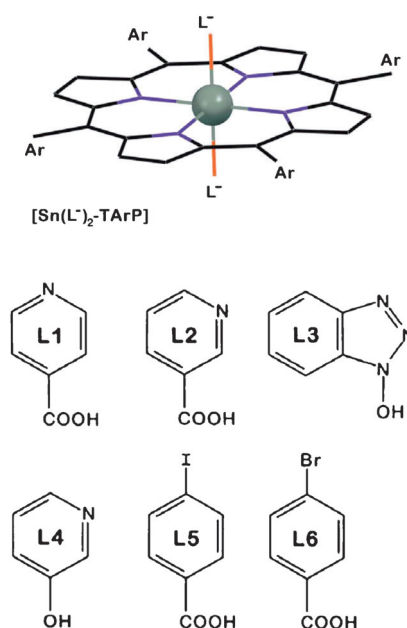


Figure 1. Layered self-assembly of tris(4-iodophenyl)-mono(4-pyridyl)-porphyrin by linear C–I...N (blue dotted lines) and perpendicular C–I...π halogen bonds (red dotted lines).^[9c] I and N sites are depicted by pink and blue colors, respectively.

In the present report, we demonstrate yet another methodology for assembling tetraarylporphyrin-based networks tessellated by intermolecular halogen bonds, which involves the use of six-coordinate tin–porphyrin complexes with axial ligands that incorporate molecular recognition functionalities suitable for halogen bonding. To this end, we have incorporated multidentate carboxylic acid or alcohol entities that may readily coordinate (in the deprotonated form) to the central tin ion as axial ligands. If the axial ligands bear additional functions such as nitrogen or halogen sites, they may engage effectively in halogen bonding with complementary sites on the periphery of the porphyrin entity. The expression of directional but relatively weak halogen bonding in the crystalline self-assembly of organic species in common reaction environments is not straightforward, in view of the competing intermolecular binding forces of similar strength, such as hydrogen bonds or π–π interactions. The latter, along with molecular-shape considerations, are of particular significance in systems with extended aromatic cores. Several theoretical investigations have probed the electrostatic potentials of a number of halogen-bonded systems, because they are a key feature affecting the formation of such interactions.^[17–19]

Crystallographic characterization of the assembly patterns formed by the six-coordinate $[(\text{Sn}^{\text{IV}}\text{-TArP})^{2+}(\text{L}^-)_2]$ (TArP: 5,10,15,20-tetraarylporphyrin; L: axial ligand) complexes throws light on the optimal supramolecular interaction of these bipyramidal metalloporphyrin units and the utilization of their halogen-bonding molecular recognition features. The porphyrins used in this study are 5,10,15,20-tetra(4'-iodophenyl)porphyrin (TAr1P), 5,10,15,20-tetra(4'-bromophenyl)porphyrin (TAr2P), 5,10,15,20-tetra(3'-pyridyl)porphyrin (TAr3P), and 5,10,15,20-tetra(4'-pyridyl)porphyrin (TAr4P). The ligand reactants are isonicotinic acid (L1), nicotinic acid (L2), 1-hydroxybenzotriazole (L3), 3-hydroxypyridine (L4), 4-iodobenzoic acid (L5), and 4-bromobenzoic acid (L6; Scheme 1). The peripheral pyridyl N sites on the porphyrin



Scheme 1. Schematic illustration of the metalloporphyrin scaffolds used in this study. Ar is 4-iodophenyl in compounds **1–4**, 4-bromophenyl in **5**, 3-pyridyl in **6** and **7**, and 4-pyridyl in **8** and **9**. L is isonicotinic acid in **1** and **5** (L1), nicotinic acid in **2** (L2), 1-hydroxybenzotriazole in **3** (L3), 3-hydroxypyridine in **4** (L4), 4-iodobenzoic acid in **6** and **8** (L5), and 4-bromobenzoic acid in **7** and **9** (L6).

and ligand components are essentially inert to potential coordination to the metal centers of another metalloporphyrin species in the reaction process (see below), due to the strong oxophilicity (and preferential affinity for the carboxy or hydroxy coordination sites of the ligands) of the tin(IV) ions; thus, the pyridyl functionalities are exposed to possible intermolecular halogen and hydrogen bonding. Correspondingly, we describe below the self-assembled architectures of the following complexes (some in their solvated forms; DMF: *N,N*-dimethylformamide): $[\text{Sn}(\text{TAr1P})(\text{L1}^-)_2]$ (**1**), $[\text{Sn}(\text{TAr1P})(\text{L2}^-)_2]$ (**2**), $[\text{Sn}(\text{TAr1P})(\text{L3}^-)_2](\text{DMF})$ (**3**), $[\text{Sn}(\text{TAr1P})(\text{L4}^-)_2](\text{DMF})_2$ (**4**), $[\text{Sn}(\text{TAr2P})(\text{L1}^-)_2]$ (**5**), $[\text{Sn}(\text{TAr3P})(\text{L5}^-)_2]$ (**6**), $[\text{Sn}(\text{TAr3P})(\text{L6}^-)_2](\text{DMF})_2 \cdot (\text{H}_2\text{O})$ (**7**), $[\text{Sn}(\text{TAr4P})(\text{L5}^-)_2]$ (**8**), and $[\text{Sn}(\text{TAr4P})(\text{L6}^-)_2]$ (**9**). Structures **1–5** exhibit prominent halogen-bonding intermolecular

interactions, which are not detected, however, in **6–9**. This diversity is interpreted below by structure and charge-density considerations. It reflects also on the delicate balance between competing halogen bonding and other noncovalent interactions during the self-assembly of the porphyrin complexes.

Results and Discussion

It has been demonstrated that halogen bonds of strength comparable to those of hydrogen bonds are attainable in crystalline systems.^[1–5,20] Most prominent intermolecular interactions have been observed between an aromatic iodine atom, highly activated by electron-attracting substituents, and strong and sterically unhindered Lewis bases. The crystal structures of tetraarylmetalporphyrins are dominated to a major extent by dispersion forces between aromatic fragments and related molecular-shape effects,^[21] and halogen and hydrogen bonding provide only a secondary cohesive contribution to the stabilization of the corresponding crystalline solids. Nevertheless, the ability to direct the supramolecular organization in crystals (in deviation from dispersion-driven packing) is associated with features of preorganization, as well as complementarity and multiplicity of the molecular recognition sites on the component building blocks. In this work, we attempted to construct crystalline multiporphyrin architectures affected by halogen bonding, utilized effectively in the crystal engineering of other systems.^[1–5] Different strategies can be applied to this end. The first one is to introduce the potential electrophilic “donor” (halogen atom) and “acceptor” (lone-pair-possessing electron-rich partner) sites on a single porphyrin macrocycle. Indeed, it has been shown that the assembly of porphyrins with mixed iodophenyl or bromophenyl and pyridyl *meso* substituents, through either I⋯N or Br⋯N halogen bonds, can be materialized successfully with both free base and metallated entities (Figure 1).^[16a,c] Manifestation of the halogen-bonding interactions occurred even without activation of the halophenyl rings by electron-attracting substituents. Herein, we extend this approach with six-coordinate metalporphyrin scaffolds by placing the electrophilic and electron-rich partners one on the tetraarylporphyrin macrocycle and the other on the axial ligand (or vice versa). Six-coordi-

nate tin–porphyrin complexes with suitably activated axial ligands were found to be perfect model compounds for demonstrating this crystal-engineering methodology.

The halogen-bonding associations in compounds **2** and **4**, with the tin–tetra(4-iodophenyl)porphyrin derivative and nicotinic acid or 3-hydroxypyridine, respectively, as the axial ligands, are illustrated in Figure 2. They represent primarily (additional interactions in **2** are discussed below) continuous self-assembly in one direction, which utilizes the laterally directed I sites on the porphyrin and the *meta*-positioned (with respect to the hydroxy or carboxy anchor) N sites on the axial ligands of adjacent porphyrin species. Every porphyrin complex is thus linked to its two neighbors by a pair of linear I⋯N_{pyridyl} interactions on each side. In the triclinic structure **4**, all of the porphyrin scaffolds along the halogen-bonded chains (propagating along the *a*–*b* axis of the crystal) are parallel to one another. In the monoclinic crystal **2**, consecutive porphyrin units along the chains (which extend along the *c* axis) are arranged in a herring-bone fashion, with the halogen-bonding pattern still preserved. In the two structures, only two of the iodophenyl residues are involved in such I⋯N halogen bonds (being thus well ordered); the other non-interacting iodophenyl substituents are directed outwards (roughly perpendicular to the chains). The I⋯N_{pyridyl} interaction distances are 3.080 and 3.086 Å in **2** and 3.122 Å in **4**, which are considerably shorter than the sum of the corresponding van der Waals radii of N and I atoms (approximately 3.5–3.8 Å).^[22] In the crystal structure of **4**, the porphyrin chains described above are aligned parallel to each other and their arrangement creates interstitial channel voids, which propagate along the *c* axis. These voids are lined with the nonbonded iodophenyl residues and accommodate molecules of the DMF crystallization solvent. The interporphyrin assembly mode of **2** and **4** into linear aggregates, through directional interactions between the aryl arms of one porphyrin unit and the axial ligands of the neighboring porphyrin entities, resembles that observed earlier in other six-coordinate metalporphyrins functionalized with hydrogen-bonding sites.^[9c,23]

In **2** and **4**, the iodine atoms not involved in the I⋯N_{pyridyl} halogen bonds, and pointing sideways with respect to the halogen-bonded chain (Figure 2), reveal partial disorder. This is indicative, perhaps, of the rather weak packing forces that they are associated with. Indeed, in **4**, these I atoms are

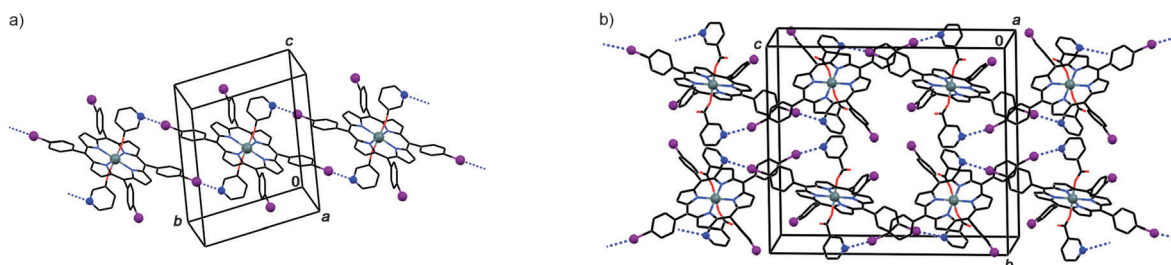


Figure 2. One-dimensional arrays of multiply halogen-bonded metalporphyrin scaffolds in a) triclinic compound **4** (the DMF crystallization solvent is omitted) and b) monoclinic compound **2**. The I⋯N_{pyridyl} halogen bonds are indicated by blue dotted lines. Note that every porphyrin unit is involved in four halogen bonds, irrespective of whether the molecules are arranged in a parallel or herring-bone manner.

surrounded by, and in van der Waals contact with, the DMF crystallization solvent trapped in the crystal lattice. On the other hand, a more detailed inspection of the intermolecular organization in **2** reveals that the interface between neighboring chains in a layer parallel to the *ac* plane of the crystal is lined with direct I...I contacts at 3.856 Å distance. (This is the shortest intermolecular I...I distance observed between the major sites of these disordered I atoms; for simplicity, longer interactions were not considered.) The layered grid-type arrangement of the porphyrin entities (Figure 3) exhib-

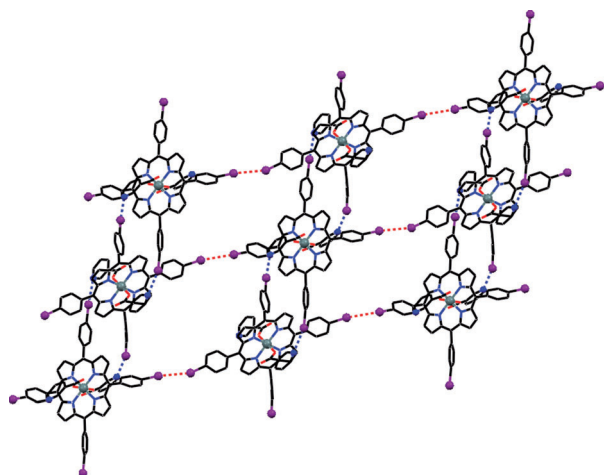


Figure 3. Two-dimensional array (**sql**) of multiply halogen-bonded metalloporphyrin moieties (4-c nodes) in **2** aligned parallel to the *ac* plane of the crystal. The I...N_{pyridyl} (along the nearly vertical direction; see Figure 2b) and I...I (along the horizontal direction at 3.865 Å) halogen bonds are indicated by blue and red dotted lines, respectively.

its two opposite edges double bridged by the I...N bonds, with the two other edges having the I...I halogen-halogen interaction (the corresponding distance being shorter than the sum of van der Waals radii of the I atoms, ≥ 4.2 Å).^[22] The topology of the two-dimensional porphyrin array thus formed has been analyzed with the TOPOS (Ver. 4.0) software, by reducing the complex structure to a simpler node-and-linker net.^[24a] Accordingly, the network depicted in Figure 3 is best described as a square layer, **sql**,^[24b] in which the porphyrin complex is considered to be four connected (4-c).

In compounds **1** and **5**, we introduced isonicotinic acid as an axial ligand. The N site is placed now in a *para* (rather than *meta*) position on the aryl residue and is thus exposed to interactions directed perpendicular to the porphyrin ring. In **1**, there are two crystallographically independent porphyrins in the asymmetric unit, with each being involved in a two-dimensional grid of halogen-bonded metalloporphyrin species (Figure 4). In such grids, every unit interacts with its four neighbors along the four lateral directions, by utilizing two I_{phenyl} and two N_{pyridyl} sites to this end. Two adjacent species in each grid are connected by a single halogen bond. The corresponding I...N distances are 3.295 Å in the centrosymmetric array and 3.150 and 3.340 Å in the other assem-

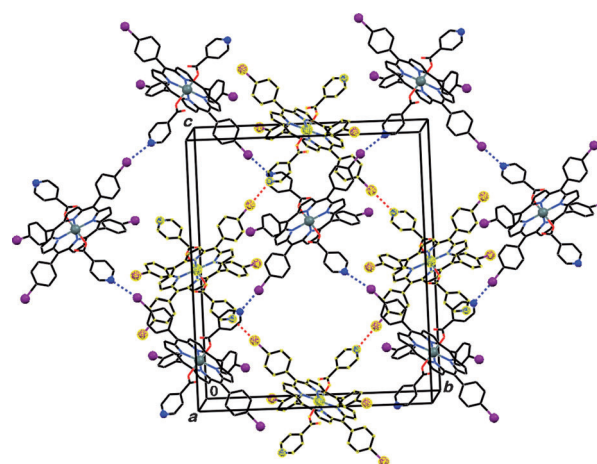


Figure 4. Crystal structure of **1**, which shows two interwoven halogen-bonded networks of the porphyrin units. The I...N halogen bonds are indicated by dotted lines; the corresponding distances are 3.295 Å for those shown by the red color in the shaded nets and 3.150 and 3.340 Å for the blue ones in the other network.

bly. The grids interweave into one another to form a flat entangled layer of the two grids, which extends parallel to the *bc* plane of the unit cell. The surfaces of these layers above and below are lined with the nonbonded I sites, which stick outwards and interdigitate between similar sites of neighboring layers stacked along the *a* axis of the crystal. The formation of the grids by nearly linear C-I...N halogen bonds is associated with a herring-bone-type arrangement of the porphyrin entities.

The topology of the interporphyrin arrangement described above and in Figure 4 is therefore best represented by twofold interpenetration of the two **sql**-type (with 4-c nodes, as in compound **2**) nets of the halogen-bonded entities.^[24] An in-depth inspection of the intermolecular contacts in **1** reveals, however, that a third (partly disordered) iodine substituent of the porphyrin units (in the unshaded network in Figure 4) is involved in yet another considerably longer I...N interaction at a distance of 3.628 Å. If this is taken into account, it changes the topology of this network from **sql** to a 2-periodic (4,4)IIb (6-c nodes) net with point symbol (4¹³.6²).^[24] This additional contact is rather close to the van der Waals limit, and the corresponding C-I...N interaction is far from linear, so the more complex description of the networking in **1** is of little relevance in the context of this paper and will not be discussed further.

A slightly distorted assembly is formed if the iodophenyl functional groups are replaced on the porphyrin macrocycle by the analogous bromophenyl residue, as in compound **5**. The bromine electrophile is characterized by lower polarizability and is less prone to engage in halogen bonds. Nevertheless, the Br...N_{pyridyl} interaction in porphyrin assemblies has been observed before,^[16a] and it is apparent in **5** as well (Figure 5). Indeed, the structure of **5** reveals a square-grid-type **sql** assembly^[24] of the porphyrin molecules located on centers of inversion, as in **1**, with roughly linear Br...N_{pyridyl} halogen bonds at 3.305 Å. The second porphyrin species of

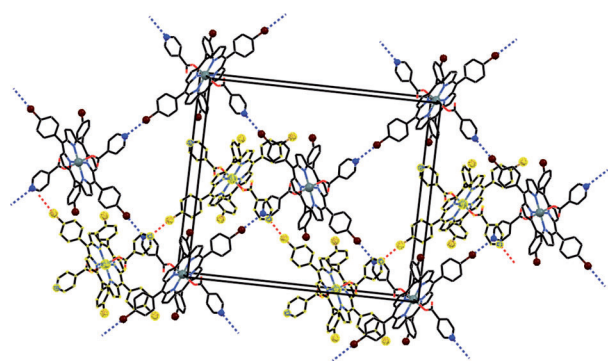


Figure 5. Crystal structure of **5**, viewed approximately down the *a* axis and with the two halogen-bonding schemes in the structure shown: the grid and the zigzag-chain (shaded) patterns. The linear Br...N halogen bonds are indicated by dotted lines; the corresponding distances are 3.156 Å for those shown by the red color in the shaded nets and 3.305 Å for the blue ones in the grid network.

the asymmetric unit associates into zigzag-chain assemblies by additional linear C–Br...N_{pyridyl} bonds at 3.156 Å through one of the bromophenyl residues and one pyridyl site. Similar chain arrays are part of the second **sql** grid in structure **1**, the formation of which didn't occur in **5** (see below). These two ensembles pack together in a tight manner, parallel to the *bc* plane, and the molecular units of the zigzag chain protrude into the interporphyrin voids of the square-grid array. The indicated Br...N distances are slightly shorter than the sum of the van der Waals radii of the two atoms (approximately 3.4 Å) and the interaction energy is estimated to be only about 9 kJ mol^{−1}.^[1–5,22,25] It is not surprising therefore that the electrostatic potential of the Br electrophile has also been utilized in **5** in competing intermolecular interactions of the Br...Br and Br...π types. Incidentally, there are additional Br...N_{pyridyl} interactions at distances of >3.5 Å from the zigzag-chain porphyrins to neighboring entities (however, being longer than the van der Waals distance, they seem to be of minor significance), which, if considered, would change the topological description from a 1D zigzag assembly along with the in-contact species to a distorted **sql** pattern, which interdigitates into the first flat **sql** net (the unshaded net in Figure 5).

The most pronounced manifestation of interporphyrin halogen bonding in this study has been observed in compound **3** with the tetra(iodophenyl)porphyrin derivative and 1-hydroxybenzotriazole as an axial ligand. The latter is characterized by an increased electron density at the N binding site, due to the presence of two additional N sites, which facilitates its direct interaction with the iodine electrophile. The self-assembly of the [Sn(TAr1P)(L3[−])₂] entities in **3** (Scheme 1) results in two-dimensional layers of the porphyrin units interconnected to one another along the four equatorial directions by nearly linear C–I...N_{triazole} halogen bonds (Figure 6). Two iodophenyl and two triazole functions of a given molecule take part in these bonds, with the I...N distance being 2.991 Å (markedly shorter than the sum of the van der Waals radii of the two atoms). Secondary I...I halo-

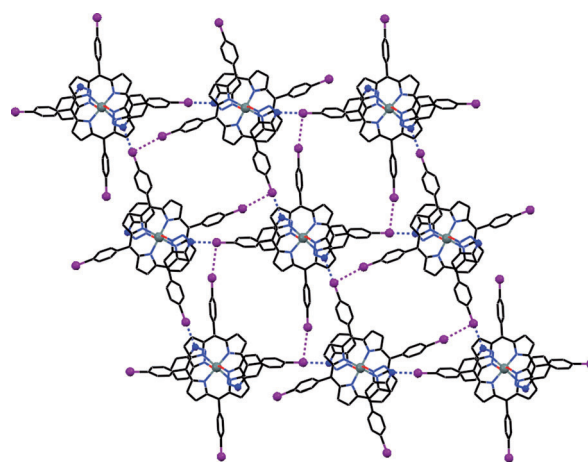


Figure 6. Supramolecular self-assembly in **3** into 2D halogen-bonding square-grid-type 'polymers'. The I...N bonds (at 2.991 Å) are indicated by blue dotted lines, whereas the I...I interactions (at 3.941 Å) are depicted by pink dotted lines. Note that every porphyrin unit is involved in four I...N bonds and four I...I contacts.

gen–halogen interactions between perpendicularly oriented C–I groups, at 3.941 Å, are also apparent within these assemblies (Figure 6). The corrugated nature of the layers thus formed allows tight stacking of the layers in the normal direction, with convex surfaces of one layer (represented by the axial ligands) fitting into the concave areas (formed by the peripheral fragments of the porphyrins) of two adjacent layers from above and below. Narrow interstitial channel voids extending along the *c* axis of the structure accommodate disordered DMF solvent. The topology of the formed network is a 2-periodic **hxl** net (the triangular lattice), in which the six-coordinate metallocporphyrin entity is considered as a 6-c node. The resulting extended grid assembly in **3** closely resembles the supramolecular organization observed earlier for the [Sn(tetra-(4-pyridyl)porphyrin)(5-amino isophthalic acid)₂] compound, which was directed in a similar way by COOH...N_{pyridyl} and NH₂...N_{pyridyl} hydrogen bonds.^[9c]

In structures **1–5** the lateral iodophenyl sites that are not involved in the linear I...N halogen bonds reveal partial disorder (particularly of the terminal iodine atoms). This provides another indication of the significance of the halogen bonds incorporating the other (well-ordered) iodine electrophiles for the intermolecular organization.

In the next step we have examined several examples of systems in which the disposition of the halogen (I or Br) electrophiles and N_{pyridyl} sites was reversed. In compounds **6–9**, the halogen sites are placed on the axial ligands (4-bromo- or 4-iodobenzoic acid), whereas the N_{pyridyl} sites are incorporated into the porphyrin macrocycle (by using the tetra(3-pyridyl)- or tetra(4-pyridyl)porphyrin scaffolds). In this alternative approach, however, the expression of the linear C–Hal...N bonds in directing the self assembly of the porphyrin complexes was considerably less effective. Thus, structure **6** can be best described as composed of linear porphyrin chains sustained by other forms of intermolecular at-

tractions that involve the halogen sites (Figure 7). In this case, the C–I group doesn't point at the N_{pyridyl} site in a linear manner (and in a direction parallel to the pyridine ring) but is oriented half-way perpendicular to the pyridyl

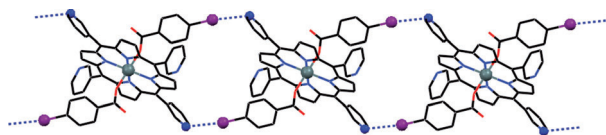


Figure 7. Linear chains of the porphyrin complexes in **6** tessellated by weak I...N interactions (3.342 Å; blue dotted lines). Dispersion forces dominate the crystal packing in the other directions.

group. This indicates an “intermediate” interaction between the C–I...N type and the C–I... π (pyridyl) type. The inclination angle between the corresponding iodophenyl and pyridyl rings is about 45° and the I...N distance is 3.342 Å.

Structure **7**, in which the *p*-iodobenzoic acid ligand was replaced by its bromo analogue, lacks any direct Br...N interaction. Instead, the crystal packing reveals secondary intermolecular Br...Br contacts at 3.943 Å (slightly longer than the sum of two van der Waals radii of bromine atoms). As commonly observed in crystal structures containing bromophenyl groups, the corresponding C–Br bonds are aligned in a nearly perpendicular orientation, which allows the electron-rich side of one bromo substituent to point at the electron-deficient pole of the other Br site (Figure 8a).^[26,27] Further efforts to probe the nature of intermolecular interactions with the same halobenzoic acid ligands but the 4-pyridyl (instead of 3-pyridyl) derivative of the tin-porphyrin compound showed that the crystal packing in the two isomorphous compounds **8** and **9** is dominated by common dispersion forces (as in many six-coordinate complexes of tetraarylmetalporphyrins), without any marked expression of specific halogen bonding of one type or another (Figure 8b).^[21,26]

As the largest contribution to halogen bonding comes from coulombic plus first-order polarization terms,^[20] we attempted, at this stage, to apply computational electrostatic considerations to sample systems in order to throw more light on the above empirical observations. The Hirshfeld surface^[28,29] is an illustration of the three-dimensional electron density of a molecule in a crystal. Mapping the Hirshfeld surface (by using CrystalExplorer^[30]) is a useful tool for understanding and visualization of intermolecular interactions. For example, Figure 9 depicts intermolecular interactions in

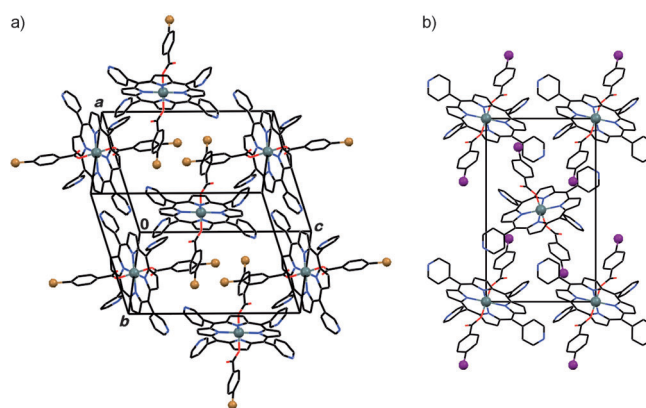


Figure 8. a) Crystal packing in compound **7**, which shows the close perpendicular approaches between the C–Br groups of neighboring molecules. b) Crystal packing in **8** (**9** is isomorphous), which resembles common crystal packing in porphyrin compounds stabilized primarily by dispersion forces.^[21,26]

structures **1** and **2**. These interactions can be analyzed by 2D fingerprint plots. In this representation, the red spots on the Hirshfeld surface evidence the appearance of close intermolecular interactions, such as hydrogen and halogen bonds, whereas areas without close contacts are shown as blue spots. Correspondingly, the halogen-bonding sites can be seen in the Hirshfeld surface as large red spots, whereas smaller red areas indicate the sites of the peripheral H atoms on the molecular surface. Two fingerprint plots are shown in Figure 9. The ones in the center reflect the total intermolecular interactions, whereas those on the right exhibit the contributions of the I...N halogen bonds only. In compound **1**, the halogen substituents contribute 27.6% to the total intermolecular surface-contact interaction, but only 2.8% of the interactions are attributable to direct I...N attractions. The tips of the spikes on the rightmost graph in Figure 9a are located at $d_i=1.80$ Å and $d_e=1.35$ Å or $d_i=$

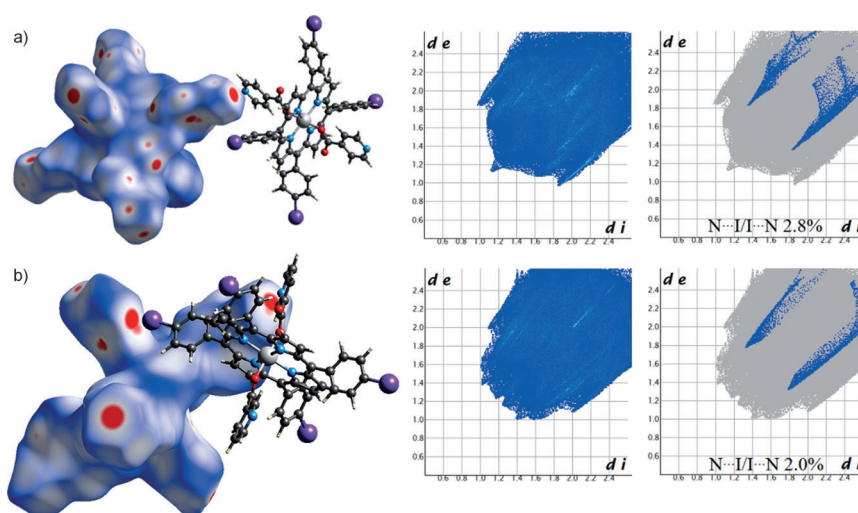


Figure 9. Calculated Hirshfeld surfaces for a) compound **1** and b) compound **2** are shown on the left side, the fingerprint plots of all of the intermolecular contacts are given in the center, and the fingerprints plots of the specific I...N interactions are given on the right for each of the two compounds.

1.35 Å and $de = 1.80$ Å, with $di + de$ representing the shortest distance between atoms inside the molecular surface and outside the surface, correspondingly. Thus, the shortest calculated interaction of about 3.15 Å is in perfect agreement with the shortest I...N bond observed in **1**. Similarly, in **2**, the halogen atoms contribute 28.5 % to the total interaction, whereas the specific I...N contacts contribute only 2.0 %. The minimal $de + di$ calculated distance between the tips of the spikes in Figure 9b is near 3.10 Å, which is in agreement with the observed 3.080 and 3.086 Å values in the crystal structure. The larger I...N halogen-bond contribution in **1** than in **2** is most probably a result of better accessibility. The calculated Hirshfeld surfaces for compounds **3** and **4** are shown in Figure 1S in the Supporting Information.

In compounds containing peripheral C_{aryl}-I or C_{aryl}-Br polarizable residues, there is a region of positive electrostatic potential at the tip/cap of this bond, known as the σ hole (the presence of positive electrostatic potential regions on the outermost portion of covalently bonded halogen atoms was confirmed by high-level theoretical calculations of electrostatic potentials in halogen-substituted compounds by Politzer and co-workers),^[17] which is prone to attractively bind to electron-rich atoms/sites (Lewis bases).^[17–19] Hence, there is preferential formation of C-I/Br...N_{pyridyl} or C-I/Br... π halogen bonds of linear or perpendicular orientation, respectively, of the interacting components (direct halogen...halogen contacts fall in the latter category). In the above context, we mapped isosurfaces of electrostatic potential for compounds **1**, **2**, **6**, and **8** with the aid of density functional theory (see the Supporting Information for details). This involved geometry optimizations, in which the starting atomic coordinates were taken from the corresponding crystal structures, followed by calculations of the molecular electrostatic potential surfaces based on both the optimized geometries and the crystallographic structural models. The calculated isosurface areas are illustrated in Figure 10 with surface contours of the molecular electronic densities, in the range of ± 0.02 electrons bohr⁻³.

As indicated in Figure 10, the iodine atoms in all four compounds are positively polarized at their cap, whereas the N_{pyridyl} sites (as well as the sterically hindered O sites) are negatively polarized. In compounds **1** and **2** and partly in **6**, these electrostatic features were well expressed by linear halogen bonds in which the electrophilic (δ^+) region of the iodine atom points toward the nucleophilic (δ^-) pyridyl nitrogen atom. The molecular electrostatic potential surface of **8** (in the crystals of which no halogen bonds of the C-I...N_{pyridyl} linear type were observed) exhibits less pronounced positive charge density at the axially oriented iodine atom (Figure 10d) than the three other molecules. Further insight is gained from computational analysis of Mulliken charge densities on the particular halogen and N atoms in question (see Figure 3S and Tables 2S and 3S in the Supporting Information). These calculations reveal that the atomic positive charge density on the iodine atom when attached to the *para* position of the axial ligand is smaller than that of an iodine atom substituted at the equatorial po-

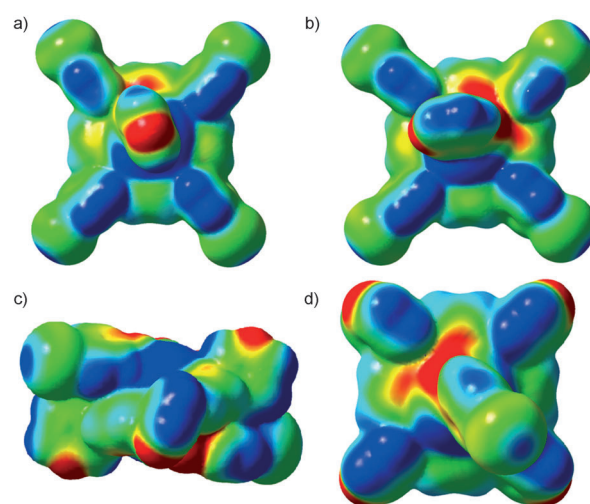


Figure 10. Electrostatic potential isosurface maps based on the experimentally derived structural models of a) **1** (with isonicotinic acid as the axial ligand), b) **2** (with the nicotinic acid ligand), c) **6**, and d) **8** (both with the 4-iodobenzoic acid ligand). The modeled charge densities are drawn at an isosurface value of ± 0.02 electrons bohr⁻³. The blue, green, and red colors represent electropositive, neutral, and electronegative regions, respectively. Similar results are also obtained if the same calculations are done by using optimized geometries (see Figure 2S in the Supporting Information).

sitions of the tetraarylporphyrin macrocycle. For example, the overall positive charge density on an iodine atom in compounds **1** and **2** is +0.26 au, whereas the positive charge density on an iodine atom in **8** is only +0.24 au (see Figure 3S in the Supporting Information). In **8**, the perpendicularly oriented axial ligand falls optimally in the ring-current region of the aromatic porphyrin, which causes a decrease of positive charge density on the halogen atom. It is reasonable to assume that the same applies to compounds **7** and **9**. The situation is different in compound **6** because the 4-iodophenyl ligand is inclined by about 45° towards the porphyrin framework, which places the terminal iodine atom in the outer region of the porphyrin ring current (Figure 7) and doesn't affect its positive charge density to the same extent as that in compounds **7–9**. Similar reasoning and ring-current effects apply to the negative charge densities of the N_{pyridyl} atoms. They increase if the N atoms fall in the ring-current region; the nitrogen negative charge density in compounds **1** and **2** is -0.54 au, whereas it is -0.52 au in compound **8**. The above considerations indicate that systems with halogen sites on the porphyrin component and accessible pyridyl sites on the axial ligand component (as in **1**, **2**, **4**, and **5**) have a priori higher odds of exhibiting directional halogen-bonding interactions than systems with reversely substituted functions (as in **7–9**). Minor fluctuations of the charge density on the interacting partners and the potential presence of competing interactions, such as hydrogen bonding, may bias the delicate balance in favor or against the expression of the directional halogen bonding in the self-assembly process.

Conclusion

The above results demonstrate new types of porphyrin-based network materials supramolecularly organized into one-dimensional and two-dimensional architectures, mainly by means of cooperative directional halogen bonding. They confirm that a concerted utilization of halogen-bonding attractions between large and rigid building blocks (such as the tetraarylporphyrins) often has adequate driving force during the nucleation stage in solution for the preferred construction of supramolecular frameworks with long-range order. Six-coordinate complexes of tin-tetraarylporphyrins with suitably functionalized sites (iodophenyl, bromophenyl, or pyridyl groups) on the porphyrin and on the axial ligand provide excellent model compounds for probing halogen-bonding interactions. Structure **3** represents an optimal realization of this crystal-engineering concept, because it reveals networking in two dimensions and the shortest linear I...N halogen bond of 2.991 Å. In this compound, the reactive N sites of the triazole axial ligand are characterized by a higher electron density than the pyridyl sites in the other analyzed compounds. Although the specific halogen bonds present only a small contribution to the total enthalpy of the intermolecular packing and are not a major cohesive factor, they can play a significant role in directing the supramolecular organization of molecular scaffolds with preorganized and sterically unhindered molecular recognition functions. The formation of network arrangements can be realized with multiply functionalized complementary components of the halogen electrophiles (even in cases in which the electrophilicity of the aromatic iodine atom is not enhanced by electron-withdrawing substituents) and electron-rich Lewis base sites. Expression of halogen bonds in porphyrin assemblies is not easy to obtain and requires careful design of the molecular scaffolds and optimal experimental conditions to avoid interference from other reagents and the dominance of competing intermolecular interactions (including features of molecular shape^[21]).

Experimental Section

Material syntheses: Full details on the preparation of materials are given in the Supporting Information. In all reactions, commercially available reagents of analytical grade were used without further purification, including the free base *meso*-tetrakis(3-pyridyl)porphyrin and *meso*-tetrakis(4-pyridyl)porphyrin. The *meso*-tetrakis(4-iodophenyl)- and *meso*-tetrakis(4-bromophenyl)porphyrin variants were prepared through common procedures of porphyrin synthesis by condensing iodobenzaldehyde or bromobenzaldehyde with hot propionic acid. In the next stage, tin insertion into the porphyrin macrocycle was achieved by treating the corresponding porphyrin derivative with tin dichloride dissolved in pyridine. The dichloride was then converted into the dihydroxide derivative by treating it with an aqueous solution of sodium hydroxide.^[9c] In the following steps, the syntheses of complexes **1–9** were carried out by treating the corresponding tin(dihydroxide)porphyrin [Sn(TArP)(OH)₂] with a stoichiometric excess of the axial ligand L in a bath reactor at 90–100 °C in an appropriate environment (DMF). The resulting products were cooled to room temperature, washed, and left for crystallization in the presence of various templating solvents.

Crystal structure determinations: The X-ray measurements (Nonius-KappaCCD (**1**, **3**, **4**, **8**, **9**) and Bruker-ApexDuo (**2**, **5–7**) diffractometers, MoK α radiation) were carried out at approximately 110(2) K on crystals coated with a thin layer of amorphous oil to minimize crystal deterioration, possible structural disorder, and related thermal motion effects and to optimize the precision of the structural results. These structures were solved by direct and Fourier methods and refined by full-matrix least-squares methods (by using standard crystallographic software: SIR97, DIRDIF-96, SHELXTL-2012).^[31a–c] All non-hydrogen atoms were refined anisotropically. The hydrogen atoms were located in idealized/calculated positions and were refined by using a riding model. Compound **3** was found to contain molecules of severely disordered DMF crystallization solvent, which could not be reliably modeled by discrete atoms. The contribution of these molecules was subtracted from the diffraction pattern by the SQUEEZE procedure and PLATON software.^[31d] Compounds **8** and **9** were found to be isomorphous, and therefore, only structure **8** has been analyzed in full detail, with structure **9** being of low quality. The crystallographic and experimental data for **1–9** are given in Table 1S in the Supporting Information. CCDC-939013 (**1**), CCDC-939014 (**2**), CCDC-939015 (**3**), CCDC-939016 (**4**), CCDC-939017 (**5**), CCDC-939018 (**6**), CCDC-939019 (**7**), CCDC-939020 (**8**), and CCDC-939021 (**9**) contain the supplementary crystallographic data for this paper. These data can be obtained free of charge from The Cambridge Crystallographic Data Centre via www.ccdc.cam.ac.uk/data_request/cif.

Acknowledgements

This research was supported by The Israel Science Foundation (grant no. 108/12).

- [1] P. Metrangolo, G. Resnati, T. Pilati, S. Biella in *Halogen Bonding: Fundamentals and Applications* (Eds.: P. Metrangolo, G. Resnati), Springer, Berlin, **2008**, pp. 105–136.
- [2] a) E. Parisini, P. Metrangolo, T. Pilati, G. Resnati, G. Terraneo, *Chem. Soc. Rev.* **2011**, *40*, 2267–2278; b) T. M. Beale, M. G. Chudzinski, M. G. Sarwar, M. S. Taylor, *Chem. Soc. Rev.* **2013**, *42*, 1667–1680; c) P. Metrangolo, H. Neukirch, T. Pilati, G. Resnati, *Acc. Chem. Res.* **2005**, *38*, 386–395.
- [3] a) M. Erdélyi, *Chem. Soc. Rev.* **2012**, *41*, 3547–3557; b) G. Cavallo, P. Metrangolo, T. Pilati, G. Resnati, M. Sansotera, G. Terraneo, *Chem. Soc. Rev.* **2010**, *39*, 3772–3783; c) A. C. Legon, *Phys. Chem. Chem. Phys.* **2010**, *12*, 7736–7747.
- [4] a) P. Metrangolo, F. Meyer, T. Pilati, G. Resnati, G. Terraneo, *Angew. Chem.* **2008**, *120*, 6206–6220; *Angew. Chem. Int. Ed.* **2008**, *47*, 6114–6127; b) G. Mínguez Espallargas, L. Brammer, P. Sherwood, *Angew. Chem.* **2006**, *118*, 449–454; *Angew. Chem. Int. Ed.* **2006**, *45*, 435–440; c) T. T. T. Bui, S. Dahanoui, C. Lecomte, G. R. Desiraju, E. Espinosa, *Angew. Chem.* **2009**, *121*, 3896–3899; *Angew. Chem. Int. Ed.* **2009**, *48*, 3838–3841; d) M. G. Sarwar, B. Dragisic, S. Sagoo, M. S. Taylor, *Angew. Chem.* **2010**, *122*, 1718–1721; *Angew. Chem. Int. Ed.* **2010**, *49*, 1674–1677.
- [5] a) H. M. Yamamoto, Y. Kosaka, R. Maeda, J. Yamaura, A. Nakao, T. Nakamura, R. Kato, *ACS Nano* **2008**, *2*, 143–155; b) L. Meazza, J. A. Foster, K. Fucke, P. Metrangolo, G. Resnati, J. W. Steed, *Nat. Chem.* **2012**, *5*, 42–47; c) Y. Lu, Y. Liu, Z. Xu, H. Li, H. Liu, W. Zhu, *Expert Opin. Drug Discovery* **2012**, *7*, 375–383; d) D. W. Bruce, P. Metrangolo, F. Meyer, T. Pilati, C. Prsang, G. Resnati, G. Terraneo, S. G. Wainwright, A. C. Whitwood, *Chem. Eur. J.* **2010**, *16*, 9511–9524; e) P. Metrangolo, G. Resnati, T. Pilati, R. Liantonio, F. Meyer, *Polym. Chem.* **2007**, *45*, 1–15; f) S. K. Chandran, R. Thakuria, A. Nangia, *CrystEngComm* **2008**, *10*, 1891–1898; g) K. Rissanen, *CrystEngComm* **2008**, *10*, 1107–1113.
- [6] a) F. Scandola, C. Chiorboli, A. Prodi, E. Iengo, E. Alessio, *Coord. Chem. Rev.* **2006**, *250*, 1471–1496; b) K. Fujiwara, T. Kurahashi, S. Matsubara, *J. Am. Chem. Soc.* **2012**, *134*, 5512–5515; c) M. Juraw,

- A. E. Schuckman, J. D. Batteas, C. M. Drain, *Coord. Chem. Rev.* **2010**, *254*, 2297–2310.
- [7] a) I. Goldberg, *Chem. Commun.* **2005**, 1243–1254; b) I. Goldberg, *CrystEngComm* **2002**, *4*, 109–116; c) I. Goldberg, *Chem. Eur. J.* **2000**, *6*, 3863–3870.
- [8] a) S. Lipstman, S. Muniappan, S. George, I. Goldberg, *Dalton Trans.* **2007**, 3273–3281; b) S. Muniappan, S. Lipstman, S. George, I. Goldberg, *Inorg. Chem.* **2007**, *46*, 5544–5554; c) S. Lipstman, I. Goldberg, *Acta Crystallogr. Sect. C: Cryst. Struct. Commun.* **2009**, *65*, m371–m373; d) S. Lipstman, I. Goldberg, *Cryst. Growth Des.* **2010**, *10*, 1823–1832; e) S. Lipstman, I. Goldberg, *Cryst. Growth Des.* **2010**, *10*, 4596–4606; f) S. Lipstman, I. Goldberg, *Cryst. Growth Des.* **2010**, *10*, 5001–5006.
- [9] a) H. J. Kim, H. J. Jo, J. Kim, S. Y. Kim, D. Kim, K. Kim, *CrystEngComm* **2005**, *7*, 417–420; b) G. J. E. Davidson, L. H. Tong, P. R. Raithby, J. K. M. Sanders, *Chem. Commun.* **2006**, 3087–3089; c) R. Patra, H. M. Titi, I. Goldberg, *Cryst. Growth Des.* **2013**, *13*, 1342–1349.
- [10] a) M. E. Kosal, J.-H. Chou, S. R. Wilson, K. S. Suslick, *Nat. Mater.* **2002**, *1*, 118–121; b) D. W. Smithenry, S. R. Wilson, K. S. Suslick, *Inorg. Chem.* **2003**, *42*, 7719–7721; c) K. S. Suslick, P. Bhyrappa, J.-H. Chou, M. E. Kosal, S. Nakagaki, D. W. Smithenry, S. R. Wilson, *Acc. Chem. Res.* **2005**, *38*, 283–291.
- [11] a) E.-Y. Choi, P. M. Barron, R. W. Novotny, H.-T. Son, Ch. Hu, W. Choe, *Inorg. Chem.* **2009**, *48*, 426–428; b) P. M. Barron, H.-T. Son, Ch. Hu, W. Choe, *Cryst. Growth Des.* **2009**, *9*, 1960–1965; c) P. M. Barron, C. A. Wray, Ch. Hu, Z. Guo, W. Choe, *Inorg. Chem.* **2010**, *49*, 10217–10219; d) B. J. Burnett, P. M. Barron, Ch. Hu, W. Choe, *J. Am. Chem. Soc.* **2011**, *133*, 9984–9987; e) B. J. Burnett, P. M. Barron, W. Choe, *CrystEngComm* **2012**, *14*, 3839–3846; f) L. D. DeVries, W. Choe, *J. Chem. Crystallogr.* **2009**, *39*, 229–240.
- [12] A. Fateeva, P. A. Chater, C. P. Ireland, A. A. Tahir, Y. Z. Khimyak, P. V. Wiper, J. R. Darwent, M. J. Rosseinsky, *Angew. Chem.* **2012**, *124*, 7558–7562; *Angew. Chem. Int. Ed.* **2012**, *51*, 7440–7444.
- [13] a) D. Feng, Z.-Y. Gu, J.-R. Li, H.-L. Jiang, Z. Wei, H.-C. Zhou, *Angew. Chem.* **2012**, *124*, 10453–10456; *Angew. Chem. Int. Ed.* **2012**, *51*, 10307–10310; b) H.-L. Jiang, D. Feng, T.-F. Liu, J.-R. Li, H.-C. Zhou, *J. Am. Chem. Soc.* **2012**, *134*, 14690–14693.
- [14] a) L. Meng, Q. Cheng, C. Kim, W.-Y. Gao, L. Wojtas, Y.-S. Chen, M. J. Zaworotko, X. P. Zhang, S. Ma, *Angew. Chem.* **2012**, *124*, 10229–10232; *Angew. Chem. Int. Ed.* **2012**, *51*, 10082–10085; b) X.-S. Wang, M. Chrzanowski, W.-Y. Gao, L. Wojtas, Y.-S. Chen, M. J. Zaworotko, S. Ma, *Chem. Sci.* **2012**, *3*, 2823–2827.
- [15] S. Motoyama, R. Makiura, O. Sakata, H. Kitagawa, *J. Am. Chem. Soc.* **2011**, *133*, 5640–5643.
- [16] a) H. M. Titi, A. Karmakar, I. Goldberg, *J. Porphyrins Phthalocyanines* **2011**, *15*, 1250–1257; b) S. Lipstman, S. Muniappan, I. Goldberg, *Cryst. Growth Des.* **2008**, *8*, 1682–1688; c) S. Muniappan, S. Lipstman, I. Goldberg, *Chem. Commun.* **2008**, 1777–1779.
- [17] a) P. Politzer, P. Lane, M. C. Concha, Y. Ma, J. S. Murray, *J. Mol. Model.* **2007**, *13*, 305–311; b) J. S. Murray, P. Lane, T. Clark, P. Politzer, *J. Mol. Model.* **2007**, *13*, 1033–1038; c) J. S. Murray, P. Lane, P. Politzer, *Int. J. Quantum Chem.* **2007**, *107*, 2286–2892; d) J. S. Murray, M. C. Concha, P. Lane, P. Hobza, P. Politzer, *J. Mol. Model.* **2008**, *14*, 699–704; e) P. Politzer, J. S. Murray, M. C. Concha, *J. Mol. Model.* **2008**, *14*, 659–665.
- [18] a) J. G. Hill, X. Hu, *Chem. Eur. J.* **2013**, *19*, 3620–3628; b) P. Politzer, J. S. Murray, *ChemPhysChem* **2013**, *14*, 278–294; c) T. Clark, M. Hennemann, J. S. Murray, P. Politzer, *J. Mol. Model.* **2007**, *13*, 291–296; d) P. Politzer, J. S. Murray, T. Clark, *Phys. Chem. Chem. Phys.* **2010**, *12*, 7748–7757; e) P. Shields, J. S. Murray, P. Politzer, *Int. J. Quantum Chem.* **2010**, *110*, 2823–2832.
- [19] a) K. E. Riley, P. Hobza, *J. Chem. Theory Comput.* **2008**, *4*, 232–242; b) K. E. Riley, J. S. Murray, J. Fanfrlik, J. Rezac, R. J. Sola, M. C. Concha, F. M. Ramos, P. Politzer, *J. Mol. Model.* **2011**, *17*, 3309–3318; c) K. E. Riley, J. S. Murray, P. Politzer, M. C. Concha, P. Hobza, *J. Chem. Theory Comput.* **2009**, *5*, 155–163.
- [20] A. Gavezzotti, *Mol. Phys.* **2008**, *106*, 1473–1485.
- [21] a) M. P. Byrn, C. J. Curtis, Y. Hsiou, S. I. Khan, P. A. Sawin, S. K. Tendick, A. Terzis, C. E. Strouse, *J. Am. Chem. Soc.* **1993**, *115*, 9480–9497, and references cited therein; b) R. Krishna Kumar, S. Balasubramanian, I. Goldberg, *Inorg. Chem.* **1998**, *37*, 541–552.
- [22] a) F. F. Awwadi, R. D. Wilett, K. A. Peterson, B. Twamley, *Chem. Eur. J.* **2006**, *12*, 8952–8960; b) A. Bondi, *J. Phys. Chem.* **1964**, *68*, 441–451.
- [23] M. Vinodu, I. Goldberg, *New J. Chem.* **2004**, *28*, 1250–1254.
- [24] a) TOPOS, Ver. 4.0: V. A. Blatov, *Struct. Chem.* **2012**, *23*, 955–963; <http://www.topos.ssu.samara.ru/>; b) M. O'Keeffe, M. A. Peskov, S. J. Ramsden, O. M. Yaghi, *Acc. Chem. Res.* **2008**, *41*, 1782–1789.
- [25] a) S. Berski, Z. Ciunik, K. Drabent, Z. Latajka, J. Panek, *J. Phys. Chem. B* **2004**, *108*, 12327–12332; b) A. Forni, *J. Phys. Chem. A* **2009**, *113*, 3403–3412; c) P. P. Zhou, W. Y. Qiu, S. Liu, N. Z. Jin, *Phys. Chem. Chem. Phys.* **2011**, *13*, 7408–7418.
- [26] F. H. Allen, *Acta Crystallogr. Sect. B: Struct. Crystallogr. Cryst. Chem.* **2002**, *58*, 380–388.
- [27] P. Dastidar, H. Krupitsky, Z. Stein, I. Goldberg, *J. Inclusion Phenom. Mol.* **1996**, *24*, 241–262.
- [28] F. L. Hirshfeld, *Theor. Chim. Acta* **1977**, *44*, 129–138.
- [29] a) M. A. Spackman, D. Jayatilaka, *CrystEngComm* **2009**, *11*, 19–32; b) M. A. Spackman, J. J. McKinnon, *CrystEngComm* **2002**, *4*, 378–392; c) R. Wang, T. S. Dols, C. W. Lehmann, U. Englert, *Chem. Commun.* **2012**, *48*, 6830–6832; d) J. J. McKinnon, D. Jayatilaka, M. A. Spackman, *Chem. Commun.* **2007**, 3814–3816.
- [30] CrystalExplorer 2.1, S. K. Wolff, D. J. Grimwood, J. J. McKinnon, D. Jayatilaka, M. A. Spackman, University of Western Australia, Crawley, Western Australia, **2007**; <http://hirshfeldsurface.net>.
- [31] a) A. Altomare, M. C. Burla, M. Camalli, G. L. Cascarano, C. Giacovazzo, A. Guagliardi, A. G. G. Moliterni, G. Polidori, R. Spagna, *J. Appl. Crystallogr.* **1999**, *32*, 115–119; b) DIRDIF-96 (A computer program system for crystal structure determination by Patterson methods and direct methods applied to difference structure factors), P. T. Beurskens, G. Beurskens, W. P. Bosman, R. de Gelder, S. Garcia-Granda, R. O. Gould, R. Israel, J. M. M. Smits, Crystallography Laboratory, University of Nijmegen, The Netherlands, **1996**; c) G. M. Sheldrick, *Acta Crystallogr. Sect. A: Found. Crystallogr.* **2008**, *64*, 112–122; d) A. L. Spek, *Acta Crystallogr. Sect. D: Biol. Crystallogr.* **2009**, *65*, 148–155.

Received: May 14, 2013

Revised: July 24, 2013

Published online: September 13, 2013